# AI-Enabled Vibration Sensing System for Early Detection of Trains at Active Highway-Rail Grade Crossings

Mohsen Amjadian, Ph.D.
Assistant Professor, Civil Engineering Department
University of Texas Rio Grande Valley

Constantine Tarawneh, Ph.D.
Director, UTCRS
Professor, Mechanical Engineering Department
University of Texas Rio Grande Valley

Md Masnun Rahman
Graduate Research Assistant
Civil Engineering Department
University of Texas Rio Grande Valley

Valik Villarreal
Undergraduate Research Assistant
Civil Engineering Department
University of Texas Rio Grande Valley

Dylan Rocha
Undergraduate Research Assistant
Mechanical Engineering Department
University of Texas Rio Grande Valley

A Report on Research Sponsored by

University Transportation Center for Railway Safety (UTCRS)

University of Texas Rio Grande Valley (UTRGV)

September 2024

**Technical Report Documentation Page**

| | | |
|---|---|---|
| 1. Report No.<br>UTCRS-UTRGV-M3CY23 | 2. Government Accession No. | 3. Recipient's Catalog No. |
| 4. Title and Subtitle<br><br>AI-Enabled Vibration Sensing System for Early Detection of Trains at Active Highway-Rail Grade Crossings | | 5. Report Date<br>September 24, 2024 |
| | | 6. Performing Organization Code<br>UTCRS-UTRGV |
| 7. Author(s)<br>Mohsen Amjadian, Constantine Tarawneh, Md Masnun Rahman, Valik Villarreal, Dylan Rocha | | 8. Performing Organization Report No.<br>UTCRS-UTRGV-M3CY23 |
| 9. Performing Organization Name and Address<br>University Transportation Center for Railway Safety (UTCRS)<br>University of Texas Rio Grande Valley (UTRGV)<br>1201 W. University Dr.<br>Edinburg, TX 78539 | | 10. Work Unit No. (TRAIS) |
| | | 11. Contract or Grant No.<br>69A3552348340 |
| 12. Sponsoring Agency Name and Address<br>U.S. Department of Transportation (USDOT)<br>University Transportation Centers Program<br>1200 New Jersey Ave. SE<br>Washington, DC, 20590 | | 13. Type of Report and Period Covered<br>Project Report<br>June 1, 2023 – August 31, 2024 |
| | | 14. Sponsoring Agency Code<br>USDOT UTC Program |
| 15. Supplementary Notes | | |

16. Abstract

Highway-rail grade crossings (HRGCs) play an essential role in ensuring the secure traversal of road users across railway tracks. However, despite their significance, they present safety challenges, particularly when trains go undetected, heightening the risk of potential collisions between the road user and train. This study aims to explore the viability of employing vibration sensors for detection and characterization of an approaching train's speed at HRGCs. The methodology involves analyzing rail vibrations and developing a time series predictive machine learning (ML) model. To accomplish this, a Finite Element (FE) model of a ballasted track railway is created in SAP2000, consisting of essential track components such as rails, sleepers, rail pads, ballast, and subgrade. The acceleration time history of the rails, induced by a moving single car, is recorded, and employed as input data for training and testing a Long Short-Term Memory (LSTM) network. The LSTM model predicts crucial parameters of the approaching train, including its location and speed. Successful prediction of these parameters is anticipated to enable the determination of the precise moment when the train reaches the HRGC, affording road users sufficient reaction time to safely traverse the railway track.

| | |
|---|---|
| 17. Key Words<br>Railroad Grade Crossings; Railroad Tracks; Vibration; Sensors; Neural Networks. | 18. Distribution Statement<br>This report is available for download from https://www.utrgv.edu/railwaysafety/research/mechanical/index.htm |

| | | | |
|---|---|---|---|
| 19. Security Classification (of this report) None | 20. Security Classification (of this page) None | 21. No. of Pages<br>22 | 22. Price |

## Table of Contents

## List of Figures



## List of Tables



## List of Abbreviations

| | |
|---|---|
| AI | Artificial Intelligence |
| HRGC | Highway-Rail Grade Crossing |
| LSTM | Long Short-Term Memory |
| ML | Machine Learning |
| RNN | Recurrent Neural Network |
| USDOT | U.S. Department of Transportation |
| UTC | University Transportation Center |

## Disclaimer

The contents of this report reflect the views of the authors, who are responsible for the facts and the accuracy of the information presented herein. This document is disseminated under the sponsorship of the U.S. Department of Transportation's University Transportation Centers Program, in the interest of information exchange. The U.S. Government assumes no liability for the contents or use thereof.

## Acknowledgements

The authors want to acknowledge the University Transportation Center for Railway Safety (UTCRS) at UTRGV for the financial support provided to perform this study through the USDOT UTC Program under Grant No. 69A3552348340.

## 1. Introduction

The U.S. rail network is the largest, safest, and most efficient railway network in the world that operates over 160,000 railway miles. It plays a pivotal role in enabling the transportation of goods and people throughout the nation; and due to this crucial function, it serves as a fundamental pillar in supporting the economic expansion of the United States [1]. On the other hand, the U.S. highway network also plays a crucial role in enabling the seamless transportation of both individuals and cargo, consisting of a sophisticated linked grid of roads that spans the entire nation. According to data from the U.S. Department of Transportation (USDOT), the average monthly traffic volume for the year 2022 exceeded 3,000 billion miles [2]. However, at the intersection of these two crucial transportation modes lies a point of concern—the Highway Rail Grade Crossing (HRGC), which are where a road or pathway intersects with a railway track [3].


**Figure 1: Photo of a simple active HRGC in Edinburg, Texas (Source: Google Maps)**

HRGCs facilitate the safe passage of vehicles, cyclists, and pedestrians across railway lines. However, they pose safety challenges due to the potential for collisions between trains and road users even when they are equipped by an active waning system as shown in Figure 1. If the road users attempt to cross the railway when a train is approaching without noticing warning signals, a catastrophic collision can occur that can lead to severe injuries or fatalities. Between 2010 and 2018, a total of 1,114 fatal crashes tragically occurred at HRGCs in the United States that resulted in the loss of 1,306 lives [4]. Over the course of eight years, there has been a significant 20% decrease in accidents related to HRGC. While this is an encouraging development, it is important

to acknowledge that the number of fatalities continues to be alarmingly high. This highlights the urgent necessity to persistently improve safety measures in HRGCs, especially in rural areas where road users mostly rely on passive warning devices and electrical power is scarce.

A viable solution to the increase of safety at HRGCs is to proactively detect the approaching trains from a distance from the road prior to their arrival at the crossing [5,6]. This approach provides road users with ample reaction time to react and pass the crossing safely. There are various methods for detecting trains before they reach a HRGC or a specific work zone. Some examples include the Automated Wayside Horn [7], the Magnetic Anomaly Detector [8], and Doppler Radar [9]. While these techniques have demonstrated considerable capability, they do possess limitations, primarily in their high cost and inability to detect an approaching train from a long distance, often limited to distances very close to the railway which are not long enough to provide a safe passage through the crossing.

The objective of this study is to assess the feasibility of using vibration sensors placed along the track for the detection and identification of approaching trains from a distance upstream. This is achieved through the data analysis of rail vibrations and the development of a time series predictive machine learning (ML) model. For this purpose, a finite element (FE) model of a ballasted track railway is created in SAP2000, including the key components of the track such as rails, sleepers, rail pads, ballast, and subgrade. The acceleration time history of the rails induced by a moving single car is recorded and then utilized as input data for training and testing a Long Short-Term Memory (LSTM) network using the Keras open-source library in Python [10]. This model is employed to predict the key parameters of the approaching train, including its location and speed. The prediction of these parameters will facilitate the determination of the exact moment when the train reaches the HRGC, providing road users with ample reaction time to safely cross the railway track.

## 2. Ballasted Track Railway Dynamic System

The dynamic interaction between a moving train and a ballasted track railway dynamic system is a complex problem which is characterized by numerous unknown parameters and uncertainties. The discussion below outlines the essential components of a simplified, yet reliable, “Ballast Model” proposed by Zhai et al. (2004), designed for the vibration analysis of a ballasted track railway subjected to a moving railcar [11].

2.1 Ballast Model Description

Figure 2 illustrates the key components of the ballast model, including the rail, rail pads, sleepers, ballast, and subgrade. The vertical deflection of the track is based on the conceptualization that the rail functions as a continuously elastic beam supported on an elastic foundation, the ballast, as initially proposed by Winkler [12]. The ballast is the most crucial component in the model, undergoing a localized large vertical deformation when subjected to the axle load transmitted through the sleepers. In addition, it undergoes a complex energy dissipation process attributed to dry friction between gravels and vibration wave radiation through the subgrade.

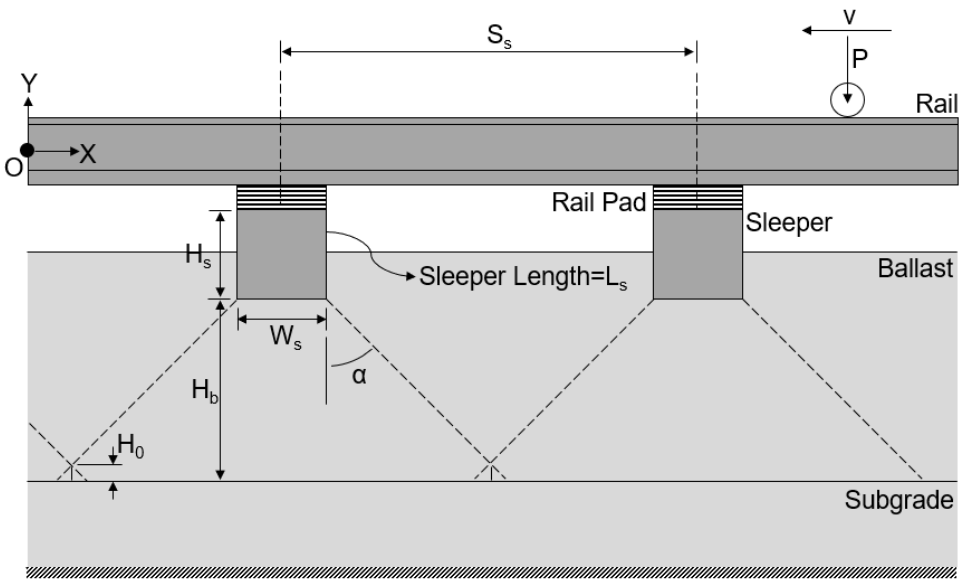


**Figure 2: Longitudinal cross-section of a ballasted track railway with its key parameters**

The axle load transmitted from the sleeper to the ballast can be approximately represented by a conical distribution characterized by the angle α as shown in Figure 2 [11,13]. Other important parameters include $S_s$, representing the center-to-center spacing between sleepers; $L_s$, the length; $W_s$, the width; $H_s$, the height of the sleeper, and $H_b$, the depth of the ballast. The height of the overlap between two adjacent conical stress distributions, denoted by $H_0$ in Figure 2, is assumed to be zero (i.e., $H_0 = 0$). Given this assumption, it can be concluded that [11]:

$$\tan(\alpha) = \frac{S_s - W_s}{2H_b} \quad (1)$$

Figure 3 shows the three-layer lumped dynamic model used in this study to describe the dynamic behavior of a ballasted track [11]. The rail and the sleeper are modeled using elastic beam elements connected through a rail pad, represented by a spring with stiffness $K_p$ and a damper with damping coefficient $C_p$. The sleeper is assumed to be rigid. The dynamic response of ballast beneath the sleeper is described by a spring with stiffness $K_b$, and the effective mass $M_b$ concentrated at the mass center of the ballast, as illustrated in Figure 3. To account for continuity and shear coupling effects among interlocking ballast granules, a spring with stiffness $K_w$ is introduced between adjacent ballast masses in the ballast model. In addition, the energy dissipation in the ballast model is considered through the inclusion of two dampers with damping coefficients $C_b$ and $C_w$, as depicted in Figure 3. The vibration of the ballast is transferred to the subgrade through a spring of the coefficient $K_s$ and a damper of the damping coefficient $C_s$.

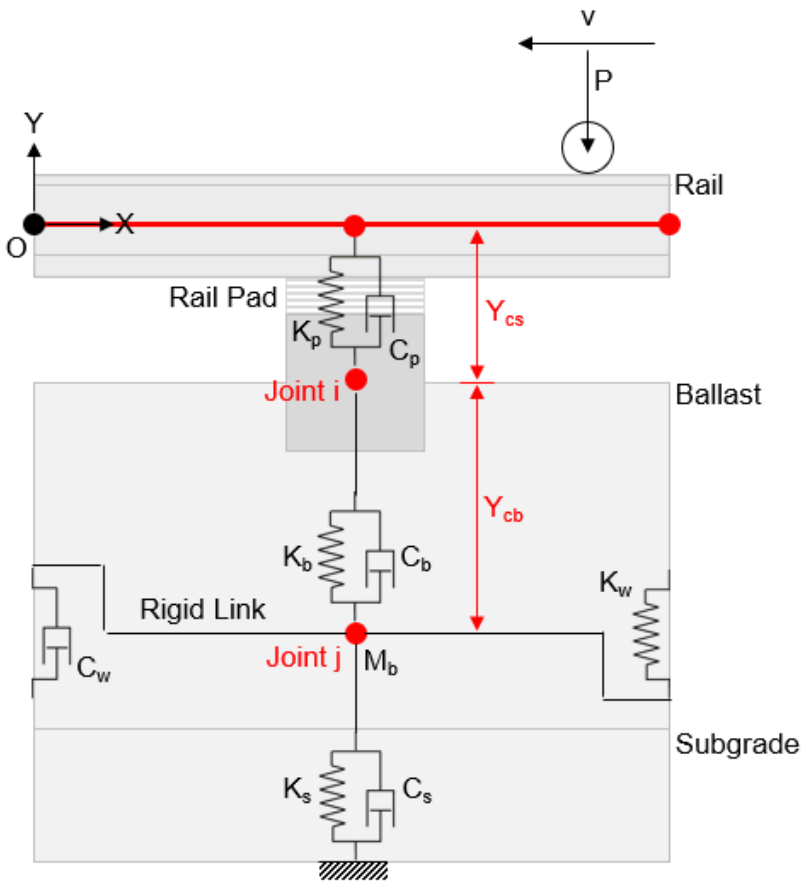


**Figure 3: Three-layer dynamic model of a ballasted track railway**

The effective mass of the ballast vibrating under one side of sleeper under a single rail can be calculated by,

$$M_b = \rho_b H_b \left[\frac{1}{2} L_s W_s + \left(\frac{1}{2} L_s + W_s\right) H_b \tan(\alpha) + \frac{4}{3} H_b^2 \tan^2(\alpha)\right] \quad (2)$$

where $\rho_b$ is the mass density of ballast. The stiffness coefficient $K_b$ of the ballast is calculated as,

$$K_b = \frac{2(L_s - W_s)\tan(\alpha)}{\ln\left[\frac{L_s}{W_s}\frac{W_s + 2H_b\tan(\alpha)}{L_s + 2H_b\tan(\alpha)}\right]} E_b \quad (3)$$

where $E_b$ is the modulus of elasticity of ballast. Furthermore, the stiffness coefficient $K_s$ of the subgrade is calculated as,

$$K_f = [L_s + 2H_b \tan(\alpha)]\,[W_s + 2H_b \tan(\alpha)]E_f \quad (4)$$

where $E_f$ is the subgrade modulus. The other parameters of the dynamic model, $K_p$, $K_s$, $C_p$, $C_b$, $C_w$, and $C_s$, are given from [11].

2.2 Ballast Model Parameters

It is assumed that the rail has the profile number 100ARA-A with a specific mass of 50 kg/m, a total height of 15.24 cm, a foot width of 13.97 cm, and a head height of 3.96 cm. The dimensions of the sleepers are $L_s$ = 2.5 m, $W_s$ = 0.2 m, and $H_s$ = 0.2 m. It is also assumed that the depth of the ballast is $H_b$ = 0.5 m and the angle of stress cone is $\alpha = 16.7°$ for $H_0 = 0$. Furthermore, it is assumed that the mass density of the ballast is $\rho_b$ = 1800 kg/m³, and the modulus of elasticity of the ballast is $E_b$ = 110 MPa. The subgrade modulus is also assumed to be $E_f$ = 90 MPa/m. Table 1 lists the values of the key parameters of the ballast model shown in Figure 3.

**Table 1: Parameters of the ballast model used in the FE analysis**

| Member | Parameter | Value | Unit |
|---|---|---|---|
| Rail Pad | $K_p$ | 65 | MN/m |
| | $C_p$ | 75 | kN·s/m |
| Ballast | $K_b$ | 100 | kN/m |
| | $C_b$ | 60 | kN·s/m |
| | $K_w$ | 78 | MN/m |
| | $C_w$ | 80 | kN·s/m |
| | $M_b$ | 450 | kg |
| Subgrade | $K_f$ | 70 | MN/m |
| | $C_f$ | 31 | kN·s/m |

## 3. Numerical Study

Figure 4 shows the configuration of the ballasted track railway and the position of a vibration sensor at $X_s$. The total length of the track is 221 m.

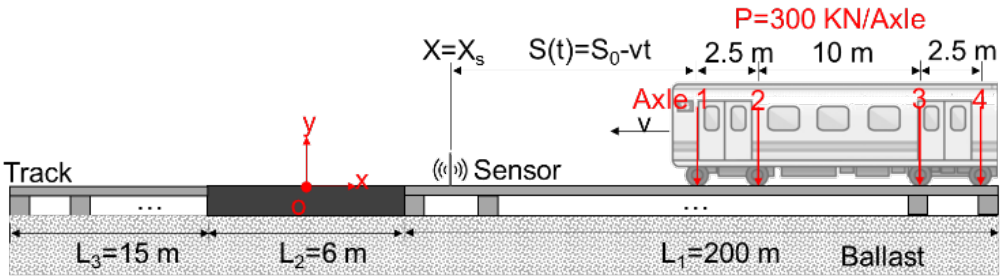


**Figure 4: Configuration of the ballasted track railway, the moving railcar, and vibration sensor**

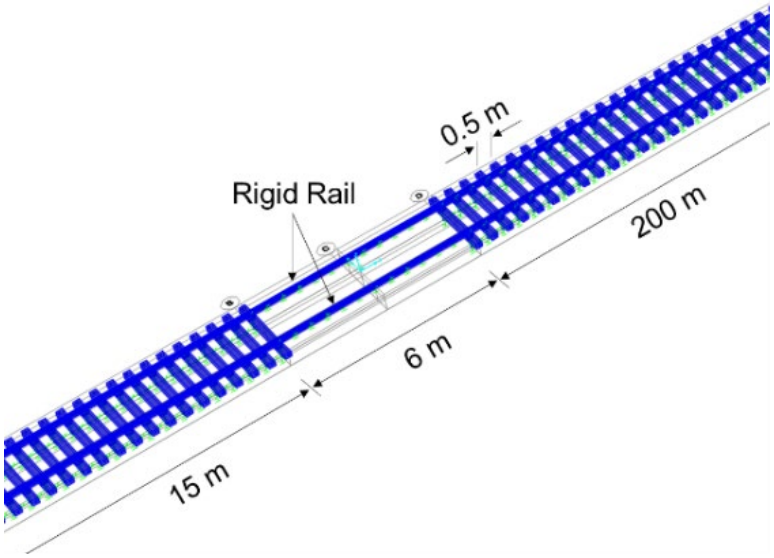


**Figure 5: FE model of a ballasted track in SAP2000**

### 3.1 Finite Element Model

In Figure 5, the FE model created in SAP2000 is depicted, where segments of the track passing through the grade crossing are represented by rigid elements supported by a series of springs and dampers, simulating a stiff subgrade. The center-to-center space between the sleepers is assumed to be $S_s = 0.5$ m. In this study, two sensors, one installed at $X_s = 3.0$ m (S1: track's end point) and

one at $X_s$ = 103 m (S2: track's midpoint) are used to measure the acceleration and deformation of the track. The dynamic load of a train with N axles moving with the constant speed v can be expressed as follows,

$$P(t) = \sum_{n=0}^{N} P_n f_n(t) \delta_n(x_n - vt) \quad (5)$$

where $P_n$ is the n-th axle load, $f_n(t) = 1 + A_n e^{i\omega_n t}$ is a harmonic function describing the vibration of suspension system of n-th axle with $A_n$ and $\omega_n$ being the amplitude and frequency parameters of the of suspension system, and $\delta_n$ is the Dirac delta function with $x_n$ being the location of the n-th axle. In this study, a single rail car with four axles (N = 4) is used for vibration analysis of the ballasted track with $P_n$ = 300 KN and $A_n$ = 0 for n = 1, 2, 3, and 4, as shown in Figure 4. The distances between the four axles are assumed to be 2.5 m, 10 m, and 2.5 m which are typical for Class I freight railcars in the US.

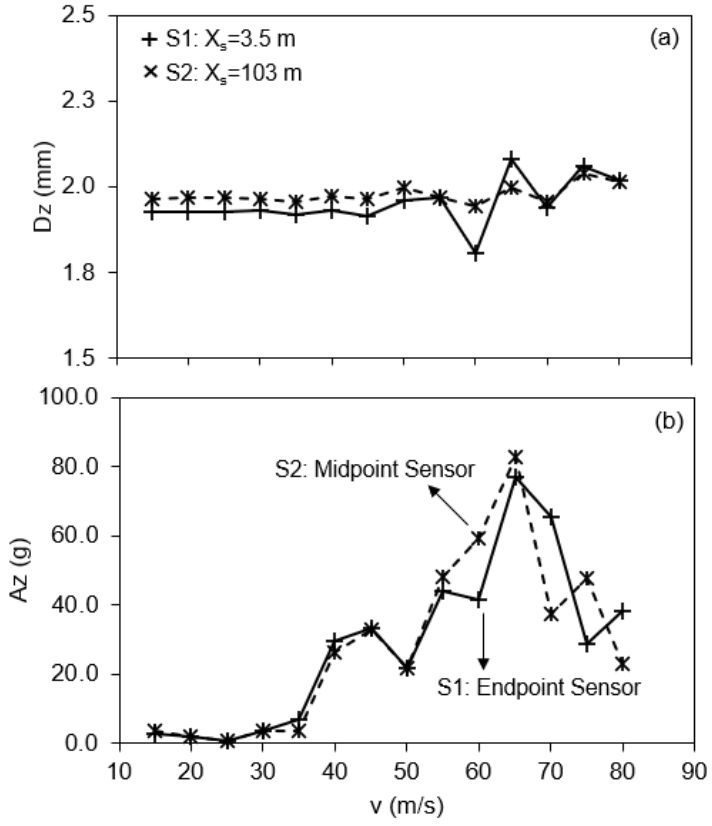


**Figure 6: Maximum (a) displacement and (b) acceleration of the ballasted track at the end and mid points of the track**

3.2 Time-Frequency Analysis

A parametric study was conducted to investigate the sensitivity of track vertical deformation and acceleration to the speed of a moving railcar, determining the critical (resonance) speed. Figure 6(a) illustrates the variation in the maximum displacement of the track at points $X_s$ = 3.0 m (track's endpoint) and $X_s$ = 103.0 m (track's midpoint) across a range of railcar speeds from 15 m/s to 80 m/s. It is observed that the track deformation, as anticipated, remains relatively insensitive to the railcar's speed, staying close to static deformation at approximately 1.9 mm. However, Figure 6(b) demonstrates that the acceleration of the track at these two points is highly sensitive to the railcar's speed for v > 30 m/s. The critical speed of the railcar is estimated to be 65 m/s, resulting in an acceleration as high as 80g for both locations.

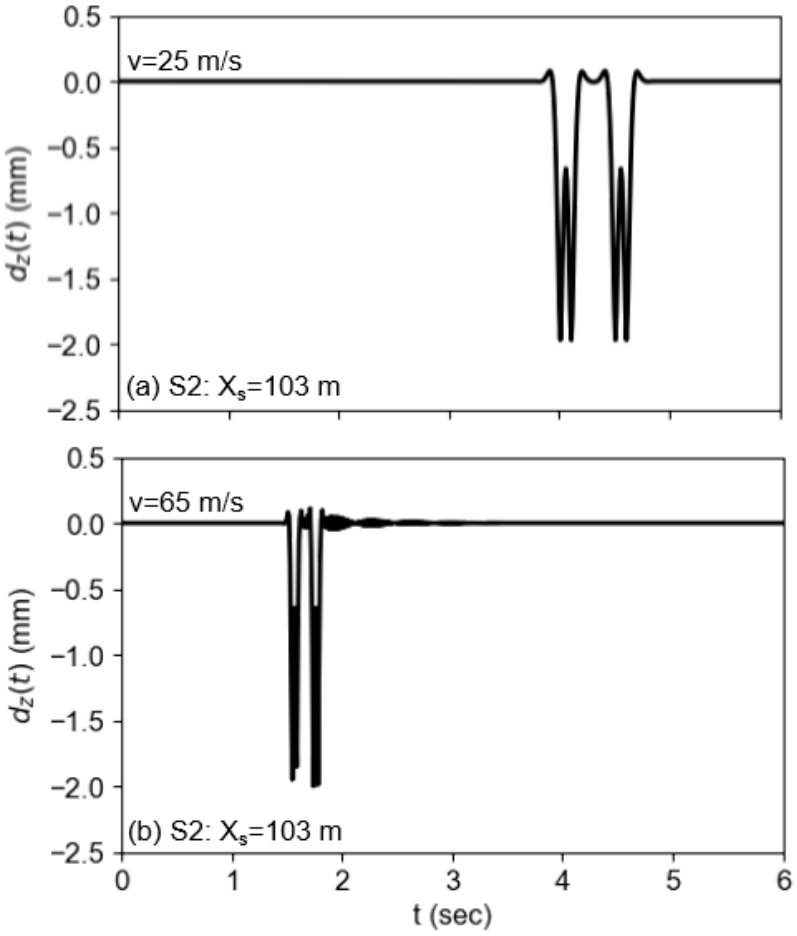


**Figure 7: Time history displacement response of the ballasted track: (a) v = 25 m/s and (b) v = 65 m/s**

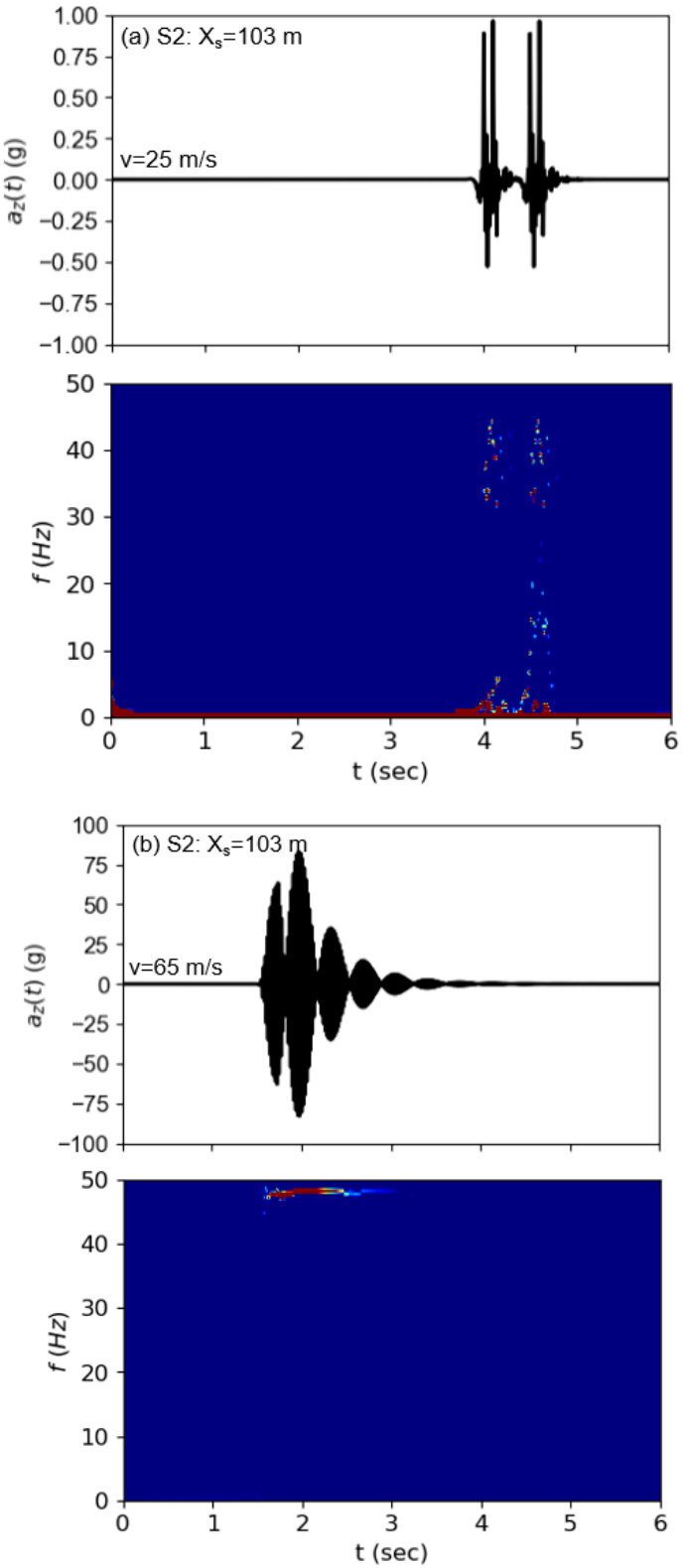


**Figure 8: Time history and Hilbert spectrum of the acceleration response of the ballasted track: (a) v = 25 m/s and (b) v = 65 m/s**

Figures 7(a) and 7(b) depict the time history of the track midpoint deformation for the speeds 25 m/s and 65 m/s (i.e., the critical speed). These plots illustrate that track deformation is highly localized, approaching zero a few meters away from the location of load. This localized effect can be attributed to high damping within the ballast. However, the acceleration response is particularly sensitive to the railcar's speed, especially at higher speeds. Figures 8(a) and 8(b) show the time history of acceleration signals recorded by sensor S2 at speeds of 25 m/s and 65 m/s, along with their respective Hilbert spectra in the time-frequency domain. The Hilbert spectrum for v = 25 m/s illustrates the distribution of signal's energy concentration over a broad frequency range from f = 10 Hz to f = 45 Hz. In contrast, for the case of v = 65 m/s, the energy is concentrated around f = 48 Hz.

## 4. Machine Learning Model

### 4.1 Moving Load Identification

The identification of a dynamic load applied to a mechanical system, utilizing the system's characteristics and response—such as the moving load of a train on a ballasted track railway—is inherently an "inverse problem".

Here, let z(t) represent the response of a linear dynamic system to the dynamic force p(t) and a zero initial condition. The relationship between these two functions in the time domain is given by the convolution integral [14],

$$z(t) = \int_0^t h(t-\tau)p(\tau)d\tau \tag{5}$$

where h(t−τ) is called the Green kernel function. This equation can be written into a dispersed matrix form in the modal domain as: $\mathbf{Z}(t)=\mathbf{H}(t)\mathbf{P}(t)$ where the elements in matrix $\mathbf{H}(t)$ are the impulse response functions. The load components can be estimated by determining the inverse of the $\mathbf{H}(t)$ matrix.

However, this would be quite challenging with the traditional methods, especially for a complex dynamic system such as a ballasted track railway [15]. To overcome this, we employe a deep learning approach based on the Recurrent Neural Network (RNN) [16]. This approach allows us to estimate the key features of a moving train load (e.g., speed, axles load, etc.) in terms of the rail's acceleration without having to derive complex formulas from physical principles.

4.2 Long Short-Term Memory (LSTM) Network

LSTM network, a specialized branch of RNN, is an advanced architecture designed to address the challenge of learning dependencies in sequence data [17]. The defining characteristic of LSTM is its capability to maintain a long-term memory, which is pivotal for applications requiring the recognition of patterns over extended time intervals, such as time-series forecasting and natural language processing [18].

The defining feature of LSTM is the cell state, $C_t$, which acts as a conduit for carrying relevant information across the sequence of data. It is accompanied by the hidden state, $h_t$, that holds the output from the LSTM cell at each time step and can be utilized for subsequent predictions or further processing [17]. The operational integrity of the LSTM is governed by three gates [19], each responsible for modulating the flow of information:

*Forget Gate ($n_t$):* This gate is essential in culling information considered as non-essential from the cell state [20]. It operates through the following equation:

$$n_t^l = \sigma\left(U_n^l h_t^{l-1} + W_n^l h_{t-1}^l\right) \tag{6}$$

*Input Gate ($i_t$):* Concurrently, the input gate evaluates new data for addition to the cell state, as determined by this relationship:

$$i_t^l = \sigma\left(U_i^l h_t^{l-1} + W_i^l h_{t-1}^l\right) \tag{7}$$

*Output Gate ($O_t$):* The output gate filters the information from the cell state to form the final output at each time step:

$$o_t^l = \sigma\left(U_o^l h_t^{l-1} + W_0^l h_{t-1}^l\right) \tag{8}$$

The cell state is updated by synergistically combining the outputs of the forget and input gates, which is succinctly expressed as:

$$C_t = n_t' \odot C_{t-1} + i_t^l \odot \widetilde{C}_t^l \tag{9}$$

The $\widetilde{C}_t^l$ symbolizes the candidate values for the cell state update [19], generated by a "tanh" layer to regulate the values within the range of -1 to 1:

$$\widetilde{C}_t^l = \tanh\left(U_c^l h_t^{l-1} + W_c^l h_{t-1}^l\right) \tag{10}$$

The output of the LSTM, the hidden state $h_t$, is computed by applying the output gate to the updated cell state, as described by:

$$h_t^l = o_t' \odot \tanh(C_t^l) \quad (11)$$

In the above equations, U and W represent the matrices of weights associated with different gates within the LSTM cell. These weights are subjected to optimization during the training process. The σ function, known as the sigmoid function, yields outputs confined between 0 and 1 and is integral to the gating mechanisms. The "tanh" function, or hyperbolic tangent, produces outputs between -1 and 1 and is utilized to modulate the cell state and the output. Finally, the sign ⊙ denotes the Hadamard product, which facilitates element-wise multiplication.

The LSTM operates in a cyclic procedure where the forget gate evaluates and filters out the redundant information from the previous cell state. Simultaneously, the input gate, in conjunction with the tanh layer, prepares new candidate values. The cell state is then updated, merging retained information and new insights. Finally, the output gate synthesizes the cell state into the hidden state, delivering the LSTM's output.

4.3 Data Collection

Upon finalizing the FE model, a rail car was subjected to multiple runs at varying speeds along the track using the moving load algorithm in SAP2000. These speeds ranged from 15 m/s to 60 m/s, increasing incrementally by 5 m/s. The acceleration responses were collected from the two distinct points on the track: $X_s$ = 3.0 m (the proximal sensor, or S1) and $X_s$ = 103.0 m (the distal sensor, or S2). The placement of these sensors aimed to discern the impact of location on capturing optimal acceleration responses, a crucial factor in determining the train's most suitable speed. The data, collected at a time step of dt = 0.01 sec, resulted in two comprehensive datasets. Each dataset consists of approximately 14,000 data points, cumulatively presenting a set of 28,000 data points for the ML model training. This approach was essential in enhancing the understanding of train dynamics on ballasted tracks.

4.4 ML Model Training and Testing

The acceleration response datasets are processed through the LSTM model. To establish a robust testing environment, data corresponding to a speed of 25 m/s was deliberately omitted from both the training and testing datasets. This specific dataset was exclusively reserved for assessing the LSTM model's performance as unseen data. The "StandardScaler" function was employed to normalize these datasets. Furthermore, an investigation was carried out to optimize the hyperparameters of the LSTM model. This optimization is focused on tuning the number of

epochs. The training regimen for the model extended over 200 epochs, with a batch size of 50. This implies that the model underwent 200 complete iterations across the training dataset, with each iteration processing batches comprising 50 data points.

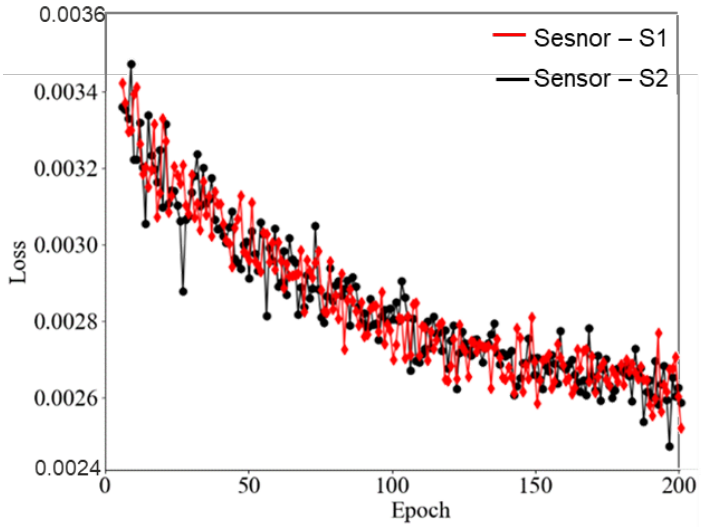


**Figure 9: Relationship between the loss parameter and epoch**

Following the LSTM model training process, the Epoch-vs-Loss graph is plotted in Figure 9, which illustrates the performance of LSTM model, based on data from sensors S1 and S2, over 200 training epochs. Loss values, indicating prediction errors, decreased from about 0.0034 to just below 0.0026, signaling the LSTM model's enhanced prediction accuracy. Both lines on the graph show expected fluctuations, with sensor S1's data displaying slightly greater variability. This visual representation confirms the LSTM model's learning efficacy as it was exposed to the acceleration data, adjusted through hyperparameter tuning, and improved steadily with each epoch. The epoch size was chosen as 150 for training the dataset by accepting Loss = 0.00265.

Figure 10 illustrates the performance of the LSTM model in terms of actual versus predicted speeds, plotted across a speed range of 15 m/s to 60 m/s. As depicted in the figure, the model yielded highly accurate training results, successfully predicting nearly every speed with precision. It is noteworthy that, due to the exclusion of data points corresponding to v = 25 m/s during training, a distinct and abrupt transition is observed between speeds of 20 m/s and 30 m/s.

After completing the training phase using the designated datasets, the remaining data—specifically, the acceleration responses corresponding to a velocity of 25 m/s—underwent a

predictive analysis. In Figure 11, it is evident that the model successfully forecasted the speed for all data points associated with sensors S1 and S2. The predicted speeds for each sensor closely matched the actual speeds, exhibiting minimal deviation from v = 25 m/s, as indicated by the small spikes observed in the graph. This precision highlights the model's effectiveness in deducing from the trained data to accurately predict speed that was not explicitly part of its training set. This indicates the robustness of the LSTM model in handling unforeseen data scenarios.

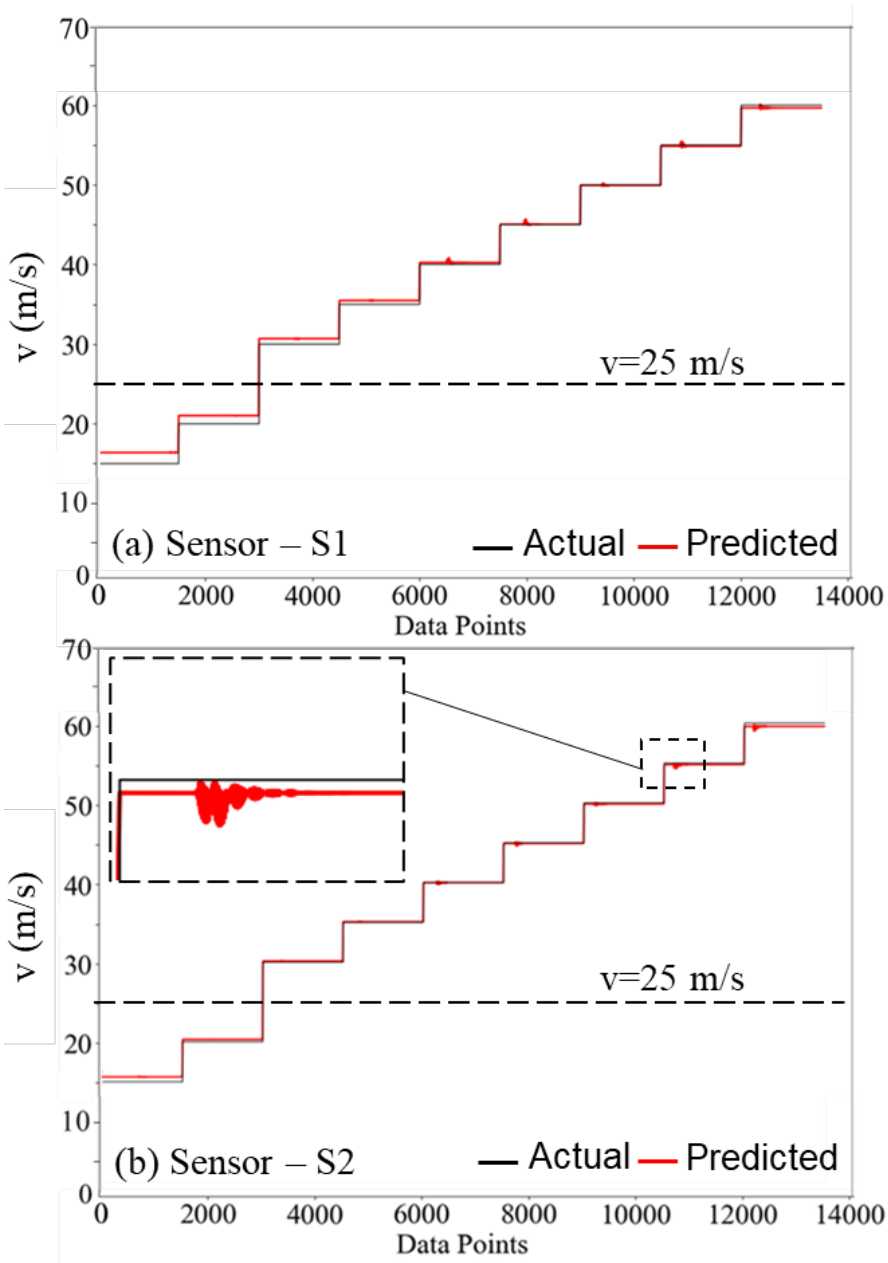


**Figure 10: Actual vs predicted graphs: (a) sensor S1 and (b) sensor S2**

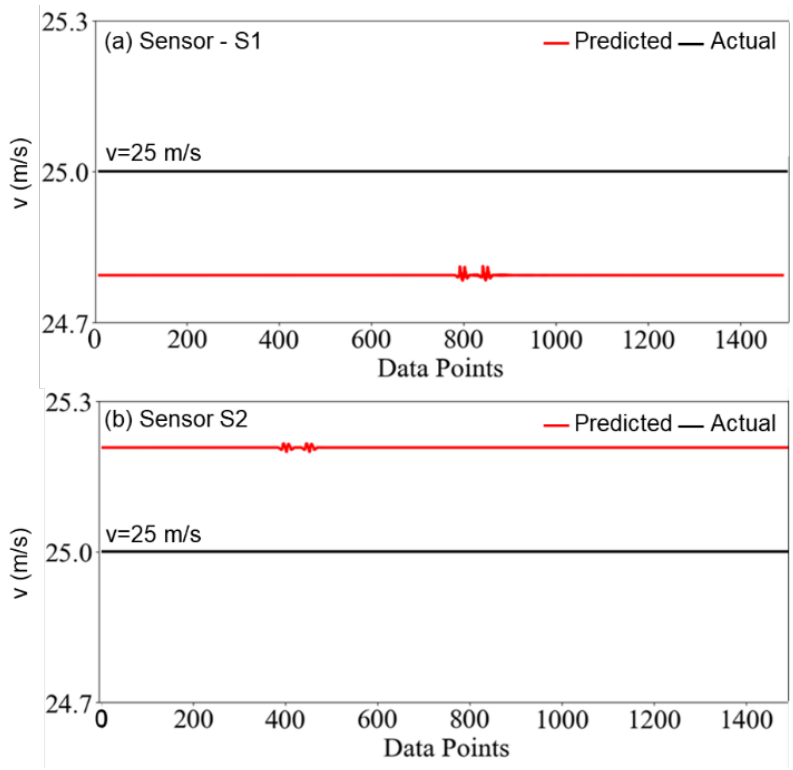


**Figure 11: LSTM model evaluation for v = 25 m/s (Unseen Data): (a) sensor S1 and (b) sensor S2**

Furthermore, the accuracy of the predictions is assessed by calculating the Mean Squared Error (MSE), Root Mean Squared Error (RMSE), and Mean Absolute Percentage Error (MAPE) based on the sensor data. Here, lower values of these metrics indicate higher accuracy. Table 2 presents the values of these metrics. For sensor S2, the MSE was 0.125, RMSE was 0.353, and MAPE was 0.014. In addition, for sensor S1, the accuracy was slightly higher, with an MSE of 0.069, RMSE of 0.262, and MAPE of 0.010. These statistics not only confirm the model's precision in prediction of train's speed but also highlight that S1 exhibited slightly superior performance in capturing and processing acceleration responses for this purpose.

**Table 2: LSTM model's testing accuracy**

| Accuracy Parameters | Sensor | |
|---|---|---|
| | S1 | S2 |
| **MSE** | 0.069 | 0.125 |
| **RMSE** | 0.262 | 0.353 |
| **MAPE** | 0.010 | 0.014 |

## 5. Conclusions

In summary, this study presents an AI-enabled vibration sensing methodology for train detection at highway-rail grade crossings (HRGCs). To conduct the vibration analysis, we have developed a finite element model of a ballasted track railway system near a grade crossing, capturing acceleration data from a moving railcar with a wide range of speed from v = 15 m/s to 80 m/s. To tackle the inverse problem of identifying dynamic loads, we have employed a deep learning approach, utilizing a Long Short-Term Memory (LSTM) network to estimate the moving railcar features (i.e., speed) based on the track's acceleration. The results demonstrate the high accuracy of the trained LSTM model in predicting the train's speed at different speeds, using acceleration data collected at two locations: the mid (S2) and end (S1) of the track. The model reliably predicted speeds, particularly the excluded 25 m/s data, demonstrating its robust generalization capabilities. The accuracy parameters—MSE, RMSE, and MAPE—confirmed the model's high predictive accuracy, with S1 slightly outperforming S2. In conclusion, our AI-enabled system offers a proactive solution for HRGC safety. By integrating vibration analysis and machine learning, it holds promise in reducing accidents especially in areas where having access to more complex train detection methods is not easy. In the next stage of this study, we aim to collect acceleration data in the field, including noise measurement, to further enhance the system's robustness and field service applicability.

## 6. References


[1] Federal Railroad Administration, 2023, "Rail Network Development."

[2] Federal Highway Administration, 2023, "Traffic Volume Trends."

[3] Khattak, A., and Lee, M., 2018, Highway-Rail Crossing Safety Improvements by Diverting Motorist to Alternate Routes, No. 26-1121-0018-007, University of Nebraska-Lincoln, University Transportation Center for Railway Safety.

[4] Das, S., Kong, X., Lavrenz, S. M., Wu, L., and Jalayer, M., 2022, "Fatal Crashes at Highway Rail Grade Crossings: A U.S. Based Study," *International Journal of Transportation Science and Technology*, 11(1), pp. 107–117. https://doi.org/10.1016/j.ijtst.2021.03.002

[5] Chen, Y., and Rilett, L. R., 2017, "Train Data Collection and Arrival Time Prediction System for Highway–Rail Grade Crossings," *Transportation Research Record*, 2608(1), pp. 36–45. https://doi.org/10.3141/2608-05

[6] Zheng, Z., Lu, P., and Tolliver, D., 2016, "Decision Tree Approach to Accident Prediction for Highway–Rail Grade Crossings: Empirical Analysis," *Transportation Research Record*, 2545(1), pp. 115–122. https://doi.org/10.3141/2545-12

[7] Raub, R. A., and Lucke, R. E., 2004, "Use of automated wayside horns for improving highway-rail grade crossing safety.", Proceeding of the Annual Meeting and Exhibit Institute of Transportation Engineers (ITE), Lake Buena Vista, FL, August 1-4, 2004.

[8] Reiff, R. P., Gage, S. E., Carroll, A. A., and Gordon, J. E., 2004, Evaluation of Alternative Detection Technologies for Trains and Highway Vehicles at Highway Rail Intersections, No. DOT/FRA/ORD-03/04, Federal Railroad Administration.

[9] Santos, J., Hempel, M., and Sharif, H., 2013, "Sensing Techniques and Detection Methods for Train Approach Detection," 2013 IEEE 78th Vehicular Technology Conference (VTC Fall), pp. 1–5. https://doi.org/10.1109/VTCFall.2013.6692407

[10] Chollet, F., 2015, "Keras.", GitHub.

[11] Zhai, W. M., Wang, K. Y., and Lin, J. H., 2004, "Modelling and Experiment of Railway Ballast Vibrations," *Journal of Sound and Vibration*, 270(4), pp. 673–683. https://doi.org/10.1016/S0022-460X(03)00186-X

[12] Frýba, L., 1995, "History of Winkler Foundation," *Vehicle System Dynamics*, 24, pp. 7–12. 10.1080/00423119508969611

[13] Ahlbeck, D. R., Meacham, H. C., and Prause, R. H., 1978, "The Development of Analytical Models for Railroad Track Dynamics," *Railroad Track Mechanics and Technology*, pp. 239–263. https://doi.org/10.1016/B978-0-08-021923-3.50017-6

[14] Liu, R., Dobriban, E., Hou, Z., and Qian, K., 2022, "Dynamic Load Identification for Mechanical Systems: A Review," *Arch Computat Methods Eng*, 29(2), pp. 831–863. https://doi.org/10.1007/s11831-021-09594-7

[15] Bengio, Y., Simard, P., and Frasconi, P., 1994, "Learning Long-Term Dependencies with Gradient Descent Is Difficult," *IEEE transactions on neural networks*, 5(2), pp. 157–166. https://doi.org/10.1109/72.279181

[16] Hochreiter, S., and Schmidhuber, J., 1997, "Long Short-Term Memory," *Neural computation*, 9(8), pp. 1735–1780. https://doi.org/10.1162/neco.1997.9.8.1735

[17] Greff, K., Srivastava, R. K., Koutník, J., Steunebrink, B. R., and Schmidhuber, J., 2016, "LSTM: A Search Space Odyssey," *IEEE transactions on neural networks and learning systems*, 28(10), pp. 2222–2232. https://doi.org/10.48550/arXiv.1503.04069

[18] Zhu, Y., Sekiya, H., Okatani, T., Yoshida, I., and Hirano, S., 2022, "Real-Time Vehicle Identification Using Two-Step LSTM Method for Acceleration-Based Bridge Weigh-in-Motion System," *Journal of Civil Structural Health Monitoring*, 12(3), pp. 689–703. https://doi.org/10.1007/s13349-022-00576-

[19] Zhou, J. M., Dong, L., Guan, W., and Yan, J., 2019, "Impact Load Identification of Nonlinear Structures Using Deep Recurrent Neural Network," *Mechanical Systems and Signal Processing*, 133, p. 106292. https://doi.org/10.1016/j.ymssp.2019.106292

[20] Sinha, A., Chorzepa, M. G., Yang, J. J., Kim, S.-H. S., and Durham, S., 2022, "Deep-Learning-Based Temporal Prediction for Mitigating Dynamic Inconsistency in Vehicular Live Loads on Roads and Bridges," *Infrastructures*, 7(11), p. 150. https://doi.org/10.3390/infrastructures7110150